

Pressure constraints on the CO₂ storage capacity of the saline water-bearing parts of the Bunter Sandstone Formation in the UK Southern North Sea

J.D.O. Williams*, S. Holloway, G.A. Williams

British Geological Survey, Environmental Science Centre, Keyworth, Nottingham,
NG12 5GG, UK

*Corresponding author (e-mail: jdow@bgs.ac.uk)

Word count, main body text: 6,556

Word count, figure captions: 588

References: 55

Tables: 2

Figures: 11

Abbreviated title: Pressure and CO₂ storage in the Bunter Sandstone

Abstract: The Bunter Sandstone Formation (BSF) in the UK sector of the Southern North Sea is thought to have a significant potential for the injection and storage of anthropogenic CO₂ within periclinal structures that lie above salt domes and pillows formed by halokinesis in underlying Zechstein strata. During the formation of the periclinal structures, the BSF and its overlying top seals were subjected to extensional stresses and in consequence are commonly cut by seismically resolvable faults that present a risk to the containment of gas and buoyant fluids such as supercritical CO₂. Although most

of the closed structures in the BSF are saline water-bearing, eight gas fields (total gas initially-in-place >72 bcm) have been discovered to date. The seismically-resolved structure of these gas fields demonstrates that two different top seals, the Haisborough Group and the Speeton Clay, can seal gas columns of up to 128 and 104 m respectively, despite the presence of faults with small displacements above the field gas-water contacts. The observed gas columns are equivalent to CO₂ columns of up to around 100 m in height. Simple geomechanical modelling suggests that existing optimally-oriented faults may dilate or be reactivated if the pore-fluid pressure increase as a result of CO₂ injection exceeds a gradient of about 13.4 MPa km⁻¹, potentially resulting in loss of storage integrity.

END

Keywords: Bunter Sandstone Formation, fault reactivation, carbon capture and storage, carbon dioxide, Southern North Sea, pore pressure, geomechanical modelling

The geological storage of CO₂ has been identified as a key option for reducing greenhouse gas emissions generated from large-scale fossil fuel combustion (IPCC 2005). In the UK sector of the Southern North Sea (SNS), the Bunter Sandstone Formation (BSF), which is of Triassic age, is perceived as having significant potential for the storage of anthropogenic CO₂ (Holloway *et al.* 2006). The BSF is folded into a series of large periclinal folds formed by post-depositional halokinesis of underlying (Permian) Zechstein Group strata. Eight gas fields with BSF reservoirs have been discovered and placed on production to date (Fig. 1), indicating that the overlying succession has the capacity to seal gases within the BSF periclinal folds, at least under favourable circumstances. Table 1 gives the depths to the producing intervals and the volumes of gas initially-in-place. An undeveloped discovery has also been made by well 42/15b-1. However, most of the periclinal folds in the BSF are saline water-bearing, most likely because of lack of gas charge (see below), and their ability to contain gases is not proven. As the periclinal folds developed their crests were subjected to extensional stresses and many of them contain crestal faults which could provide leakage pathways to overlying permeable strata and ultimately to the seabed. The potential for leakage along these faults is considered to be one of the key factors in the CO₂ storage prospectivity of the BSF periclinal folds that requires further investigation (Noy *et al.* 2012). Consequently, we have assessed the potential for faults in the BSF to act as CO₂-leakage pathways by (a) investigating the gas columns and pressures retained by seismically resolved faults in the BSF-reservoired gas fields and (b) by modelling the likely effects of realistic reservoir pressure increases that would result from CO₂ injection, on faults in the saline water-bearing periclinal folds.

Geological setting

Detailed accounts of the structure, stratigraphy and petroleum system of the SNS are given by Cameron *et al.* (1992) and Underhill (2003). The UK sector of the SNS forms the westernmost part of the Southern Permian Basin, a major sedimentary basin extending from Eastern England to the eastern Polish border (Doornenbal & Stevenson 2010). The generalised stratigraphy of the region is shown in Figures 2 and 3. Permian and younger strata were deposited above a partially-eroded substrate of Carboniferous and older rocks, which include Upper Carboniferous gas-prone source rocks. Following deposition of the Lower Permian Rotliegend Group, which includes the prolifically gas-bearing Leman Sandstone Formation, the Zechstein Group, a cyclic carbonate–evaporite sequence, was deposited. This is more than 1000 m thick in the central parts of the basin. The overlying Triassic succession is marked by a return to non-marine clastic deposition, which formed the Triassic Bacton and Haisborough Groups. The lower fine-grained part of the Bacton Group is ascribed to the Bunter Shale Formation, while the upper, sand-dominated, fluvial sediments comprise the BSF.

Throughout most of its distribution, the BSF reservoir is overlain by the Haisborough Group, a thick sequence of predominantly red mudstones that contains up to three halite-bearing members: in ascending order the Röt, Muschelkalk and Keuper halites. Rhaetic and Jurassic strata consisting predominantly of mudstones and interbedded thin limestones assigned to the Penarth, Lias, West Sole and Humber groups commonly overlie the Haisborough Group, although they have been removed by erosion at the Late Cimmerian Unconformity (LCU) in many areas. Thin and probably impersistent sandstones in the Penarth Group are the first strata above the

BSF that are likely to have good reservoir properties. Above the LCU, the mudstone-dominated Cromer Knoll Group is overlain by the Chalk Group, which is in turn overlain by Cenozoic strata in the eastern part of the UK sector (Lott & Knox 1994). The distribution and thickness of the topseal formations above the BSF are described by Cameron *et al.* (1992) and Heinemann *et al.* (2012): total seal thickness is commonly in excess of 500 m. In the eastern part of the UK sector, on the Cleaver Bank High, the LCU cuts down through the BSF and overlying strata such that the early Cretaceous Speeton Clay Formation rests unconformably on the BSF.

Structural setting

The Sole Pit Trough (Fig. 1) was the centre of subsidence and deposition in the UK sector of the Southern Permian Basin from late Triassic to early Cretaceous times. Its western margin was controlled by a zone of en echelon faults (the Dowsing Fault Zone) that cuts the Rotliegend and older succession (Stewart & Coward 1995). However, most of these faults do not actually cut the younger post-Zechstein basin-fill, because the Zechstein evaporites act as a detachment between the underlying Rotliegend and older strata, and the overlying Bacton Group and younger rocks, and evaporites infill the fault topography. The post-Zechstein strata are cut by a separate but genetically related zone of faults known as the Dowsing Graben System that in places overlies, but elsewhere is geographically displaced by up to 3 km from the Dowsing Fault Zone (Stewart & Coward 1995). The SW end of the Dowsing Graben System, in the area adjacent to the Hewett Field, is directly linked to the underlying Dowsing Fault Zone by major faults that cut both the pre- and post-Zechstein succession.

On the northern margin of the SNS basin, the post-Zechstein succession is cut by a set of faults, the North Dogger Fault Zone (Griffiths *et al.* 1995), that are genetically similar to those of the Dowsing Graben System. The North Dogger Fault Zone similarly overlies, but is detached by the Zechstein evaporites from a series of small faults in the Rotliegend and older strata.

Development of anticlines and periclinal

Halokinesis in the basin centre (Griffiths *et al.* 1995; Stewart & Coward 1995), the area to the east of the Dowsing Graben System, south of the North Dogger Fault Zone and north of the diapiric salt limit shown by Taylor (1984), resulted in the folding of the BSF and other post-Zechstein strata into a series of elongate anticlines and domes. These typically trend approximately NW–SE (Wall *et al.* 2009). Lateral displacement on the North Dogger Fault Zone and the Dowsing Graben System accommodated the tectonic shortening caused by sliding of the post-Zechstein cover above the zone of detachment in the Zechstein evaporites. This is thought to have begun as early as late Carnian to Norian times, during deposition of the Triton Formation (Allen *et al.* 1994). Halokinesis was intermittent during the Mesozoic, and a later, major episode occurred in Early to Mid-Eocene times in the Silverpit Basin (Fig. 1), which continued progressively rather than episodically into the Oligocene, and was terminated prior to deposition of the (Cenozoic) Nordland Group (Underhill 2009). In this area the Zechstein salt may have been mobilised by high heat flow adjacent to early Palaeogene dykes that cross the area. This may have resulted in salt flow away from the dykes, and development of linear salt-cored anticlinal ridges between the

dykes and their coincident synclines caused by salt withdrawal (Underhill 2009). The Caister B Field structure (Ritchie & Pratsides 1993) shows evidence of episodes of structural growth that both pre-date and post-date the LCU.

Inversion of the Sole Pit Trough, expressed as episodic inversion events, took place from late Cretaceous to Oligocene times (Glennie & Boegner 1981; Van Hoorn 1987). Structural closure in the Hewett and Orwell BSF-reservoired gas fields resulted from late Cretaceous compressional folding (Cooke-Yarborough & Smith 2003), probably related to the Sole Pit inversion.

The seal potential of faults cutting the BSF may in general terms be related to the degree and intensity of deformation, and to the orientation of the faults with respect to the *in situ* stress. As the BSF is commonly overlain by a considerable thickness of fine-grained caprocks, only faults with large displacements are expected to provide a risk of up-dip cross-fault migration because smaller faults juxtapose the BSF against impermeable overburden strata. In addition, faults with larger displacements are also likely to have thicker damage zones, with the possible exception of wide deformation band formation at low throws in coarser-grained facies (Childs *et al.* 2007). Major faults cutting both the pre- and post-Zechstein successions can therefore be expected to form a higher risk for CO₂ storage, while those faults accommodating extension over the periclinal culminations, and not extending great distances upwards into the post-BSF caprock succession (and are therefore presently inactive), are expected to be more capable of withstanding excess fluid pressures.

Charging of the gas fields in the BSF

The source rocks for gas in the SNS are predominantly coals of the Upper Carboniferous Conybeare Group (Westphalian) Coal Measures (Underhill 2003). To reach the BSF, gas generated from these coals first needed to migrate through the Rotliegend strata, represented in the western half of the basin by the Leman Sandstone Formation and in the eastern half of the basin by the mudstone-dominated Silverpit Formation. It would then have had to pass through the Zechstein evaporites, the Brockelschiefer and the Bunter Shale (Fig. 3), which represent a significant barrier to migration as they form a highly effective seal to the gas fields in the Leman Sandstone Formation. Consequently relatively few Triassic gas fields have been discovered in the UK SNS to date.

The BSF-reservoired Esmond, Forbes, Gordon, Caister B and Hunter fields, which lie in the part of the basin affected by halokinesis, are not filled to their respective spill points (Bifani 1986; Ketter 1991; Ritchie & Pratsides 1993). Three hypotheses have been put forward to explain this. First, salt withdrawal may have allowed local, intermittent, short-lived or weak primary gas migration via temporary pathways through the Zechstein Group and (via faults or fractures) through the Bunter Shale to the BSF (Fisher 1984), or re-migration from breached Leman Sandstone Formation or Carboniferous reservoirs. Second, in the Silverpit Basin area where these fields are found, fracturing, initiated by the intrusion of Palaeogene igneous dykes may have provided a mechanism by which gas could have migrated through the underlying seals (in this area the Silverpit Formation, Zechstein Group and Bunter Shale Formation) that have otherwise prevented gas migration to the BSF (Underhill 2009). There is a good correlation between the locations of Tertiary dykes and the salt-withdrawal

synclines adjacent to the Esmond, Forbes and Gordon fields (Brown *et al.* 1994; Wall *et al.* 2009). Thirdly, the large periclinal folds formed by halokinesis may have been at an immature stage of development at the time that gas was migrating through the Zechstein Group and Bunter Shale Formation. Ketter (1991) considers that the Esmond, Forbes and Gordon fields may have been charged in mid-Triassic times, during the initial stages of the halokinesis that formed the periclinal folds in which they occur. Charging then ceased but the anticlines in which these fields are found subsequently developed much larger closures as a result of further (Cenozoic) salt movement. A similar explanation is provided for the incomplete charging of the Caister B dome (Ritchie & Pratsides 1993). Sequential structural restoration might provide a means by which to further investigate the extent of structural closure in relation to the perceived timing of gas charge in the under-filled fields. If balanced models are able to reconcile the volumes of gas initially-in-place with the extent of structural closure prior to the main phase of halokinesis (timing of migration) it would provide evidence in favour of lack of charge rather than poor seal quality.

In the Hewett Field, which lies outside the area of halokinesis (Fig. 1), gas migration may have occurred via faults such as the Dowsing and South Hewett faults that cut the entire Permian and Mesozoic succession. Gas supply was sufficient to fill the BSF reservoirs in both the Hewett and Little Dotty fields to their spill points.

In the Orwell Field, which is in the main area of halokinesis, and not filled to its spill-point, it is possible that migration of gas to the BSF may be related to the approximately coeval reactivation of the existing fault on the northern margin of the field and creation of the structural closure during Late Cretaceous compression.

These hypotheses provide logical explanations for the lack of full gas charge in the BSF gas fields in the area of detached post-Rotliegend strata and the absence of gas charge in many of the BSF periclinal structures. The presence of the Röt Halite Member over much of the basin makes it less likely that small-offset faulting (including faults below seismic resolution) or fracturing of the overburden allowed wholesale gas leakage from the structures. This is because thick halite beds are likely to deform plastically under stress, undergoing brittle fracturing only in the very shallow subsurface (Warren 2006), except in rare situations where strain rates are very high (Davison 2009). Small fractures in halite are also likely to reseal by a combination of flow and pressure solution creep (Warren 2006). Except where it is removed by the LCU along the eastern and southern margins of the UK sector, there is no evidence of discontinuity in the Röt Halite over the non-gas bearing structures, caused by either erosion or salt-flow-induced breaching. Nevertheless, the possibility that gas migration into the BSF could have been more widespread, and that gas retention could have been limited by either poor capillary sealing, or by networks of sub-seismic fractures in the caprocks, cannot be conclusively ruled out.

As far as the authors are aware, no seismic anomalies suggestive of thermogenic gas leakage (such as bright-spots or gas chimneys) similar to those observed in the Netherlands sector of the SNS (Schroot & Schüttenhelm 2003; Schroot *et al.* 2005) have been recorded above either the BSF gas fields or the water-bearing structures in the UK SNS to date.

Seal capacity of the Haisborough Group and Speeton Clay Formation

The topseal capacity of the Solling, Röt and Muschelkalk caprocks above the BSF have been measured in well P15-14 in the Netherlands sector of the SNS (Spain & Conrad 1997), and in the Mercia Mudstone Group in the onshore Willow Farm borehole near Nottingham, UK (Armitage *et al.* 2013). These strata are the distal and proximal lateral equivalents respectively of the Haisborough Group in the UK sector of the SNS.

Measured porosities in the caprock in the P15-14 well range from 0.70 to 5.4% with vertical permeabilities ranging from 0.002 to 0.240 mD (Spain & Conrad 1997). The majority of samples from the Solling, Röt and Muschelkalk have micro- to sub-microporous pore geometries. The results of mercury-injection capillary-pressure tests on a core sample from the Solling Claystone, immediately above the BSF, indicate a gas-water capillary displacement pressure of 4.688 MPa. Using the water and gas pressure gradients at the P15-14 well, this core sample would be able to retain a gas column of 594 m. For comparison, it is expected that CO₂ column heights of 70–540 m could be retained by the onshore Mercia Mudstone Group strata, based on measurements of samples taken from the Willow Farm borehole (Armitage *et al.* 2013).

It is thought that the above measurements are likely to provide a conservative guide to the seal potential of the Haisborough Group in much of the UK sector, because the Röt Halite Member immediately overlies the Solling Claystone in many UK offshore wells and the Muschelkalk and Keuper Halite Members are present higher in the Haisborough Group over parts of the UK sector (Cameron *et al.* 1992). These halites

are likely to enhance the capillary sealing qualities of the Haisborough Group where present. Seal integrity in the East Irish Sea Basin has been shown to be excellent where the Triassic reservoirs are overlain by halite-dominated intervals in the Haisborough Group equivalent Mercia Mudstone Group (Seedhouse & Racey 1997).

The gas fields in the BSF prove that the Haisborough Group is capable of sealing some significant gas columns, though these do not approach the likely gas column heights that could be retained if the seal quality were equal to, or better, than observed in the Solling in the Netherlands P15-14 well. The maximum gas column height observed in the BSF in the UK sector was 128 m, in the Hewett Field (Cooke-Yarborough 1991). The equivalent CO₂ column height, estimated using the methodology of Naylor *et al.* (2011), gas composition data from Cumming and Wyndham (1975) and field data from Cooke-Yarborough (1991), is 102 m. This estimate assumes an interfacial tension ratio of 0.5 and neglects possible contact angle changes. The initial pressure at the crest of the gas reservoir was 9.38 MPa (Cooke-Yarborough & Smith 2003), 1.13 MPa above hydrostatic.

The Speeton Clay Formation, of Ryazanian to Albian age, is the primary seal around the eroded margins of the BSF. It consists predominantly of silty mudstone, with occasional thin, very-fine grained sand-rich beds at its base. No capillary entry pressure tests are available from the Speeton Clay. However, a gas column height of approximately 102 m is observed in the Orwell Field, where the BSF is sealed by the Speeton Clay. The overpressure exerted by the gas column is 1.11 MPa, calculated using available pressure data from well 50/26a-D1.

Effect of faulting on gas containment in the BSF

Eight fields are producing, or have produced, gas from the BSF in the UK sector of the SNS: Esmond, Forbes, Gordon, Hunter, Caister B, Orwell, Hewett and Little Dotty (Fig. 1). The wireline log response of the BSF and over- and underlying strata in the different field areas is shown in Figure 3. The Orwell, Hewett and Little Dotty fields occur where the reactivation of faults may have provided migration routes for Carboniferous-sourced natural gas through the underlying Zechstein Group and Bunter Shale (Yielding *et al.* 2011).

The seismically resolvable structure of Hewett, Little Dotty, Hunter and Orwell, as imaged by 3D seismic reflection data, is investigated below. The Esmond, Forbes, Gordon and Caister B fields are described as gas pools occurring in unfaulted anticlines in the BSF (Bifani 1986; Ketter 1991; Ritchie & Pratsides 1993) and consequently were not considered further in this part of the study.

In addition to the producing fields, a further BSF gas accumulation was proved by well 42/15b-1, and is imaged clearly by an amplitude anomaly on seismic data near to the top BSF reflector (DECC 2008). Similarly to the gas fields in the Esmond area, the accumulation is pooled in a simple anticline which is not filled to its structural spill-point. Gas in place is calculated to be 0.65 bcm (23 bcf), and the immediate seal is provided by the Solling Claystone and Röt Halite Member of the Haisborough Group (DECC 2008).

The Hewett Field: Blocks 48/28, 48/29, 48/30, 52/04, 52/05.

The Hewett Field lies about 16 km off the Norfolk coast in Quadrants 48 and 52 (Fig. 1). It is approximately 29 km long and up to 5 km wide. Structurally, it comprises a NW–SE trending anticline bounded to the SW by the South Hewett Fault and to the NE by the North Hewett Fault, a splay of the Dowsing Fault Zone. It has three gas-bearing reservoirs, the highest of which is the BSF, known at Hewett as the Upper Bunter reservoir (Cooke-Yarborough & Smith 2003). The crest of this reservoir lies at 792.5 m (2600 ft) and it was initially filled near to spill point, with a 128 m (420 ft) gas column. The initial reservoir pressure was 9.39 MPa (1362 psia) at 884 m TVDSS. It was normally pressured prior to production, lying on a water gradient to surface of 0.01 MPa/m (0.46 psi/ft). The reservoir gas gradient averaged 0.0016 MPa/m (0.07 psi/ft).

The log response of the Bacton Group at the Hewett Field is shown in Figure 3, where the Haisborough Group is seen to form the primary seal to the BSF reservoir. The trapping mechanism in the main Hewett Field is entirely structural, the anticline being thought to have developed contemporaneously with normal faulting, in Upper Cretaceous times (Cooke-Yarborough & Smith 2003). Figure 4 superimposes the approximate location of the initial gas-water contact (GWC) of the Hewett Field on a seismic amplitude variance map of the top BSF surface in the Hewett area. The field spill point is either defined by, or lies very close to, the labelled faults (A), while the only other faults that cut the top of the gas reservoir, apart from antithetic faults associated with the North Hewett Fault, lie towards the SE end of the field, labelled (B).

Figure 5a presents a seismic profile through the faults at (A) and (B), with the line of section shown in Figure 4. These faults appear to approach, and may well reach, the seabed. It is possible, that the faults marked as (A) and/or the North and South Hewett faults provided a leakage pathway for natural gas during or after gas emplacement; whereas the faults marked as (B) are sealing faults if, as interpreted, they cut the reservoir above the GWC (it should be noted that the gas column height is reduced at the location of the (B) faults due to a depression in the top BSF surface).

The Little Dotty Field: Block 48/30.

The Little Dotty Field (Cooke-Yarborough & Smith 2003) lies 5 km to the NE of Hewett in Quadrant 48, and comprises Rotliegend (Leman Sandstone Formation) and BSF reservoirs. The Haisborough Group forms the immediate seal to the BSF reservoir, and the trap is formed by a NW–SE oriented anticline within a tilted fault block, closed by dip to the NW, SW and SE. The NE margin of the field is formed by the Dowsing Fault (part of the Dowsing Fault Zone which in this area also forms the SW margin of the Dowsing Graben System) which cuts the BSF and all overlying strata up to, or close to, seabed. Across this fault the BSF is juxtaposed against Jurassic Lias Group and/or Humber Group strata which provide a cross-fault side-seal to the gas (Fig. 5b). The Little Dotty Field also appears to be affected by crestal faulting (in the Haisborough Group), shown on Figures 4 and 5b as (C), which has not adversely affected the height of the gas column, as the field was initially filled to its spill point, with a potential migration pathway towards the NW. Gas shows have been observed in well 48/30–6 within the same fault block some 1.7 km NW of the Little Dotty Field.

The Orwell Field: Block 50/26.

The Orwell Field (Fig. 1) lies within an inversion anticline, formed by the contractional reactivation of existing Permian–Triassic and Jurassic extensional faults during the Late Cretaceous (Underhill *et al.* 2009). The structure of the field is shown in Figure 6a. Erosion at the LCU has removed all Jurassic strata, all of the Haisborough Group and part of the BSF, such that the remaining BSF is now overlain by the Speeton Clay Formation (Figs 3, 6b). An estimated 8 bcm (282 bcf) of recoverable natural gas was initially in place (DECC 2004), demonstrating the sealing capacity of the Speeton Clay Formation in this area. Seismic interpretation suggests that the initial GWC does not correspond with the lowest closing contour. It is assumed that the inverted Orwell fault defining the NW limit of the field provided the means for gas migration to BSF level, due to breaching of the underlying Zechstein Group which is inferred to have prevented the migration of gas to Triassic traps elsewhere in the area.

To the north of the main Orwell fault, and over to the east of the field, the BSF is eroded at the LCU such that the Bunter Shale Formation lies directly beneath the unconformity (Fig. 6b). Several small-offset, but vertically extensive faults cut the BSF and overlying seal above the GWC (Fig. 6b). Some of these faults extend vertically into the Neogene succession where they cut the Mid-Miocene unconformity, but it is unclear whether they extend into younger strata or to the seabed.

The Hunter Field: Block 44/23.

The Hunter Field is located within UK Quadrant 44 (Fig. 1). Structurally similar to the other fields in the area, the Hunter gas accumulation is trapped in a simple four-way dip anticline, and is not filled to its structural spill-point. The Solling Claystone and Röt Halite Member of the Haisborough Group form the immediate topseals. A crestal extensional fault is observed on 3D seismic data (Fig. 7), extending almost to the top of the Röt Halite Member, a feature typical of many of the non-gas bearing structures in the region. That the field was not initially filled to its structural spill-point is thought to reflect the relationship between the timing of structural growth and migration of gas from the Carboniferous source rocks, as in the nearby Caister B Field (Ritchie & Pratsides 1993).

Summary conclusions from gas fields

Seismically detectable faults are shown to cut the reservoir and much of the overlying succession in at least four of the eight BSF gas fields. Of these, the simple structure of the Hunter Field is most typical of the non-gas bearing structures created by halokinesis. The BSF gas fields basinward of the Dowsing Fault Zone are not filled to spill point, almost certainly because they were not fully gas-charged.

Gas column heights in both the faulted and unfaulted BSF fields are considerably lower than those that their unfaulted Haisborough Group seals are likely to be able to retain. The faulted overburden in fields with Haisborough Group top seals sustained pressures of up to approximately 1.13 MPa above hydrostatic, while the faulted

Speeton Clay Formation top seal over the Orwell Field sustained overpressure of approximately 1.11 MPa above hydrostatic.

CO₂ containment in non-gas bearing structures

Unfaulted structures

In unfaulted traps, CO₂ will be contained provided the lower of either the capillary entry pressure to CO₂ or the fracture pressure is not exceeded. From a fracture-generation perspective, the maximum sustainable reservoir pressure could be assumed to be close to the leak-off pressure (LOP), the pressure at which fracture initiation occurs (Bell 1995), though a safety margin below this pressure is likely to be required for CO₂ storage. Noy *et al.* (2012) present a graph of LOP against depth to seabed for the UK sector of the SNS. This includes data from all stratigraphic intervals, to a depth of 3000 m. There is considerable variation in LOP vs. depth. This is partly due to some of the leak-off tests included in the dataset not having been taken all the way to leak-off, and probably partly to variations in the *in situ* minimum horizontal stress and rock strength in the various locations and lithologies tested. At the depths currently of interest for CO₂ storage (>800 m) the majority of LOP measurements lie above a gradient to seabed of around 17 MPa km⁻¹. The hydrostatic pressure gradient is 10.07 MPa km⁻¹, and therefore the likely pressure increase that can be sustained is less than 7 MPa km⁻¹. An unfaulted pericline with its crest at 800 m below seabed is likely therefore to be able to sustain a maximum reservoir pressure of 13.6 MPa (a pressure increase above hydrostatic of about 5.5 MPa) without fracturing.

The capillary seal potential of the Solling Claystone in the Netherlands P15-14 well to gas, is about 4.7 MPa at a depth of 3140 m (Spain & Conrad 1997). Both the fracture and the capillary sealing pressures could easily be exceeded during CO₂ injection (Heinemann *et al.* 2012; Williams *et al.* 2013), necessitating the requirement for careful pressure control.

Faulted structures

Many of the saline water-bearing periclinal structures within the BSF are cut by seismically resolved faults (Bentham *et al.* 2013). In some cases these cut the reservoir and penetrate the entire sealing succession to reach the seabed. It is possible that these may slip or their permeability may be enhanced under the increased reservoir pressures resulting from CO₂ injection. However, some of the periclinal structures contain faults that are more subtly expressed and do not cut both the reservoir and the entire sealing overburden. Figure 8a illustrates one such structure, consisting of two separate closures connected by a saddle/common spill-point. The elongate south-eastern closure is clearly cut by two crestal extensional faults that are mapped along the fold axis, geometrically similar to the fault that cuts the BSF in the Hunter Field, albeit extending to shallower depths. Although very little offset is observed along the faults at the level of the BSF and the Haisborough Group, they can be mapped on 3D seismic data (Figs 8b, 8c). Such faults cut a large part of the sealing succession, and probably continue upwards to shallower depths and higher stratigraphic levels as fractures (rock discontinuities on which shear displacement is not observed) or faults with sub-seismic displacements. There is a risk that these faults might dilate or

propagate further through the sealing strata if subjected to reservoir pressure increases during CO₂ injection.

The Hunter, Orwell, Little Dotty and Hewett fields are all cut by faults above their GWCs. In the Orwell Field, there is a fault very close to the crest of the field (Fig. 6a). RFT data indicate that this fault sustains an overpressure (above hydrostatic) of approximately 1.1 MPa. This is the largest overpressure sustained by a fault in the BSF gas fields, because the faults in the Hewett Field are located on the field's margins where the gas column height is lower than at its crest, and the Little Dotty and Hunter fields have significantly smaller gas columns.

It is considered unlikely that the small-offset faults in the periclinal will pose a significant risk to CO₂ storage at low reservoir overpressures, similar to those observed in the BSF gas fields, on two grounds. Firstly, similar faults do not appear to have affected natural gas containment in the faulted BSF fields. Secondly, the shale gouge ratio in the faults is likely to greatly exceed the 20% threshold that is characteristic of sealing faults (Yielding *et al.* 1997) because the thickness of both the Haisborough Group and Speeton Clay top seals greatly exceeds the observed fault offsets in most of the periclinal.

Geomechanical modelling of fault failure pressure

Regional stress field

The orientation of the maximum horizontal stress (S_{Hmax}) is approximately NW–SE in the basement rocks of many parts of NW Europe (Heidbach *et al.* 2008), and analysis of borehole breakouts in 81 wells indicates the S_{Hmax} orientation is parallel to this onshore in the UK (Evans & Brereton 1990). A similar, NNW–SSE, orientation of S_{Hmax} has been derived from 26 stress measurements taken in the onshore UK Coal Measures (Cartwright 1997).

However, Hillis & Nelson (2005), citing amongst other evidence the variable borehole breakout orientations in the region, suggested that the stress regime in the post-Zechstein succession of the Central North Sea and surrounding areas including the UK SNS, is effectively decoupled from that in the Early Permian and older succession by the Zechstein evaporites. The Triassic Muschelkalk has been identified as a décollement horizon in the Eastern Jura Mountains of Switzerland (Becker *et al.* 1987), de-coupling the near-surface stress field from that in the crystalline basement, demonstrating the potential of evaporitic strata to detach the stress conditions of overlying successions. It has also been suggested that where such detachment occurs, salt diapirism may affect stress orientations in the detached cover, such as in the Danish and Norwegian sectors of the Central North Sea (Ask 1997; Fejerskov & Lindholm 2000). Analysis of borehole breakouts from the (post-Zechstein) Lias and Haisborough Groups in well 43/12–1, drilled into the crest of the non-gas bearing structure in the area of structural detachment east of the Dowsing Graben System (Fig. 9), supports both these hypotheses. The breakouts indicate that along the structural axis, the orientation of S_{Hmax} in the post-salt succession is approximately ESE. Although stress orientations are only available for one well over the structure, they compare with the axial stress orientations observed in the Ekofisk Field in the

Central North Sea, where measured stress orientations are non-uniform across a large structural dome formed by halokinesis in the underlying Zechstein (Teufel 1991). In contrast, breakouts occurring in the pre-salt succession in 43/12–1 suggest an approximately NW S_{Hmax} orientation (Fig. 9), consistent with the NW–SE regional trends in NW Europe (Heidbach *et al.* 2008). However, further analysis of *in situ* stress orientations in the pre- and post-salt succession in the area of halokinesis is needed in order to clarify whether there are consistent differences between the present-day horizontal stress orientations above and below the Zechstein salt and where any transition to the NNW–SSE orientation of S_{Hmax} observed in the UK onshore area takes place. In particular, it seems probable that the onshore stress regime might apply to the whole succession in the area of hard-linked tectonics on the southern margin of the SNS basin and SW of the Dowsing Fault Zone, and consequently might be applicable to the Hewett and Little Dotty fields which lie immediately west of the zone of detachment in the SNS.

Hillis & Nelson (2005) cite evidence that the vertical stress is the principal stress in the cover rocks of the Central North Sea, and suggest that a normal faulting regime predominates as a result of detachment, itself likely due to the effect of halokinesis. By analogy, we consider that the vertical stress in the post-Zechstein succession in the central part of the SNS is likely to be the principal stress, at least over the crests of the periclinal.

Geomechanical modelling

Simple geomechanical modelling was undertaken to estimate the likely increase in reservoir pore fluid pressure that would be required to cause frictional failure, leading to reactivation, dilation or propagation of pre-existing faults and fractures in the BSF that penetrate into, or through its cap rock.

The parameters used (Table 2) are taken primarily from leak-off pressure (LOP) data from the SNS (Noy *et al.* 2012), which almost all fall between a (lithostatic) gradient of 22.5 MPa km⁻¹ and a minimum pressure gradient of 13.7 MPa km⁻¹. Given that some of the lower values in the LOP data shown by Noy *et al.* (2012) may be from tests not fully taken to leak-off, or from tests in fractured or faulted rocks, a LOP gradient of 16.9 MPa km⁻¹ is probably conservative. The magnitude of S_{Hmax} is far less well-constrained, but by analogy with the Central North Sea is assumed here to be lower than the vertical stress because a normal-stress regime predominates in the post-Zechstein cover rocks (Hillis & Nelson 1995).

In a CO₂ storage scenario, elevated pore pressures will act to reduce the effective stress (and consequently the frictional resistance) acting along a fault plane. The coefficient of friction of a fault (μ) is the ratio of the shear stress relative to the effective normal stress acting on the fault. Faults with low frictional strength have low μ values compared to faults with higher frictional strength. Samuelson & Spiers (2012) show that the coefficient of friction of artificially-created fault gouge derived from the Bunter Sandstone and its caprock in the Netherlands sector of the SNS varies between end member values of 0.61 for quartz-rich reservoir rock gouges and 0.47 for those derived from clay-rich caprock. A μ value of 0.56, equal to that of a simulated fault gouge containing a 50/50 weight percent mixture of both BSF and Haisborough

Group equivalent rocks (Samuelson & Spiers 2012), was used in the modelling, because it is thought likely to be representative of the gouge in the small-offset faults that affect the top of the BSF and its immediate caprocks, as this would be expected to contain a mixture of both quartz and clay minerals. A conservative assumption of our geomechanical model is that optimally oriented pre-existing faults are present in the BSF and its overburden, with respect to the *in situ* stress conditions. Therefore, providing our assertion that the vertical stress is the principal stress component is valid, and the μ value used is realistic, the results provide the lower bound to the safe permissible pressure rise that could be tolerated during CO₂ injection in a faulted structure, without compromising storage integrity through fault reactivation. Non-optimally oriented faults would require greater stresses to reactivate.

A series of Mohr-circle diagrams were produced in order to determine the pore pressure gradient that would lead to failure of a pre-existing, optimally-oriented fault, given the initial stress conditions and assumptions listed in Table 2. Figure 10 plots effective normal stress (σ_n normal stress minus pore pressure) against shear stress (τ) at three depths (1000, 2000 and 3000 m) to investigate the pore fluid pressure rise required to cause failure of a pre-existing, optimally oriented fault, utilising both the Coulomb and Coulomb-Plasticity failure envelopes (Morone 1995). The Coulomb-Plasticity failure envelope is applicable to faults with thick gouge zones (Morone 1995), which may be clay-rich, and have a reduced frictional strength relative to those from granular materials. The results of Samuelson & Spiers (2012) show that saturation of clay-rich gouges with brine results in weakening of faults, whereas saturation of the quartz-rich (reservoir) gouges does not. The appropriate frictional strength envelope for faults affecting the uppermost part of the BSF and its

immediately overlying topseal may fall somewhere between the two shown in Figure 10.

The modelling determines that at a depth of 1000 m, a pore fluid pressure rise of only 3.3–3.9 MPa could be sufficient to cause frictional failure of a pre-existing fault if it is optimally oriented, depending on the failure criterion used. This can be expressed as a pore fluid pressure gradient of 14 MPa km⁻¹ assuming the Coulomb failure criterion, or 13.4 MPa km⁻¹ assuming that Coulomb-Plasticity failure criterion applies. This may be considered to approximate the elevated injection pressures that may be achieved without compromising storage integrity through reactivation and dilation of existing faults. The pressure gradients, the SNS LOPs and the overpressures exerted by both the Hewett and Orwell gas field columns at their respective reservoir depths are shown in Figure 11. It is interesting to note that the lowermost LOP values fall very close to, or between, the Coulomb fault failure pressure gradients, suggesting that these lower measurements might have been influenced by existing fractures, which may be either optimally or non-optimally oriented.

Conclusions

At least four of the eight gas fields in the BSF in the UK sector of the SNS are cut by seismically-resolvable faults above their GWCs. These faults vertically seal natural gas, and can be expected to seal equivalent column-heights of supercritical CO₂ of up to approximately 100 m. This is far less than the likely seal capacity of unfaulted overlying Haisborough Group strata, which, by analogy with measurements taken in the Netherlands sector of the SNS, could retain gas columns heights of almost 600 m.

Geomechanical modelling suggests that optimally-oriented pre-existing faults in the post-Zechstein succession of the SNS may be reactivated if pore fluid pressures are increased above a pressure gradient of 13.4 MPa km^{-1} . This provides a safe working pressure of up to ~ 1.3 times the hydrostatic pressure gradient, if optimally-oriented faults are suspected to be present. However, although it would be prudent to avoid reactivating existing structures, it should be noted that reactivation of a given fault will not necessarily cause it to act as a conduit for upward fluid flow (Bjørlykke *et al.* 2005). Accurate determinations of the maximum horizontal stress magnitude and orientation could greatly improve the estimated limiting pressure gradient. Consequently, a detailed analysis of *in situ* stress conditions involving the analysis of stress orientation and magnitude from well data (Zoback *et al.* 2003), and a subsequent analysis of the potential for faults to be reactivated (Morris *et al.* 1996; Streit & Hillis 2004) is recommended during site appraisal. Given the results of the simple geomechanical modelling outlined here, it is concluded that careful consideration should be given to the elevated pressures that would result from injection and storage of CO_2 in the BSF periclinal. This could be estimated from dynamic simulation of CO_2 injection, while coupled reservoir simulation and geomechanical modelling may be used to further address the geomechanical integrity of potential storage sites.

Acknowledgements

The authors are extremely grateful to: IHS for permission to publish the SNS LOP data, PGS for providing full access to the SNS MegaSurvey data and permission to

publish SNS MegaSurvey seismic reflection data in UK Quadrant 44, Tullow Oil plc for permission to publish seismic reflection data from the Hewett, Little Dotty and Orwell fields and WesternGeco for permission to publish seismic reflection data in UK Quadrant 43. We also thank Andy Kingdon of BGS for advice on the breakout analysis. This publication has been produced with support from the BIGCCS Centre, performed under the Norwegian research program Centres for Environment-friendly Energy Research (FME). This paper is published with the permission of the Executive Director, British Geological Survey (NERC).

References

- Allen, M.R., Griffiths, P.A., Craig, J., Fitches, W.R. & Whittington, R.J. 1994. Halokinetic initiation of Mesozoic tectonics in the southern North Sea: a regional model. *Geological Magazine*, **131** (94), 559–561.
- Armitage, P. J., Worden, R.H., Faulkner, D.H., Aplin, A.C., Butcher, A.R. & Espie, A.A. 2013. Mercia Mudstone Formation caprock to carbon capture and storage sites: petrology and petrophysical characteristics. *Journal of the Geological Society, London*, **170**, 119–132.
- Ask, M.V.S. 1997. *In situ* stress from breakouts in the Danish Sector of the North Sea. *Marine and Petroleum Geology*, **14**, 231–243.
- Becker, A., Blümling, P. & Müller, W.H. 1987. Recent stress field and neotectonics in the Eastern Jura Mountains, Switzerland. *Tectonophysics*, **135**, 277–288.

Bell, J.S. 1995. In situ stresses in sedimentary rocks (part 1): measurement techniques. *Geoscience Canada*, **23** (2), 85–99.

Bentham, M.S., Green, A. & Gammer, D. 2013. The occurrence of faults in the Bunter Sandstone Formation of the UK sector of the Southern North Sea and the potential impact on storage capacity. *Energy Procedia*, **37**, 5101–5109.

Bifani, R. 1986. Esmond Gas Complex. *In*: Brooks, J., Goff, J.C. & van Hoorn, B. (eds) *Habitat of Palaeozoic Gas in N.W. Europe*, Geological Society, London, Special Publications, **23**, 209–221.

Bjørlykke, K., Høeg, K., Faleide, J.I. & Jahren, J. 2005. When do faults in sedimentary basins leak? Stress and deformation in sedimentary basins; examples from the North Sea and Haltenbanken, offshore Norway. *AAPG Bulletin*, **89** (8), 1019–1031.

Brown, G., Platt, N.H. & McGrandle, A. 1994. The geophysical expression of Tertiary dykes in the southern North Sea. *First Break*, **12**, 137–146.

Cameron, T.D.J., Crosby, A., Balson, P.S., Jeffery, D.H., Lott, G.K., Bulat, J. & Harrison, D.J. 1992. *The Geology of the Southern North Sea*. United Kingdom Offshore Regional Report. British Geological Survey and HMSO, London.

Cartwright, P.B. 1997. *A review of recent in-situ stress measurements in United Kingdom Coal Measures strata*. In: Sugawara, K. & Obara, Y. (eds) Proceedings of the International Symposium on Rock Stress, Kumamoto, Japan, 7–10 October 1997, 469–474.

Childs, C., Walsh, J.J., Manzocchi, T., Strand, J., Nicol, A., Tomasso, M., Schöpfer, M.P.J. & Aplin, A.C. 2007. Definition of a fault permeability predictor from outcrop studies of a faulted turbidite sequence, Taranaki, New Zealand. In: Jolley, S.J., Barr, S.J., Walsh, J.J. & Knipe, R.J. (eds) *Structurally Complex Reservoirs*, Geological Society, London, Special Publications, **292**, 235–258.

Cooke-Yarborough, P. 1991. The Hewett Field, Blocks 48/28-29-30, 52/4a-5a, UK North Sea. In: Abbotts, I.L. (ed.) *United Kingdom Oil and Gas Fields, 25 Years Commemorative Volume*, Geological Society, London, Memoir 14, 433–442.

Cooke-Yarborough, P. & Smith, E. 2003. The Hewett fields: Blocks 48/28a, 48/29, 48/30, 52/4a, 52/5a, UK North Sea: Hewett, Big Dotty, Little Dotty, Della, Dawn and Delilah fields. In: J.G. Gluyas & H.M. Hichens (eds) *United Kingdom Oil and Gas Fields, Commemorative Millennium Volume*, Geological Society, London, Memoir 20, 731–739.

Cumming, A.D. & Wyndham, C.L. 1975. The geology and development of the Hewett Gas-Field. In: Woodland, A. (ed.) *Petroleum and the Continental Shelf of North-West Europe: Volume 1 Geology*, Applied Science Publishers Ltd., Barking, 313–326.

Davison, I. 2009. Faulting and fluid flow through salt. *Journal of the Geological Society, London*, **166**, 205–216.

DECC 2004. UK Petroleum data CD.

<http://www.databydesign.co.uk/energy%5Cukdata/index.htm>

DECC. 2008. Relinquishment Report. Blocks 42/10 and 42/15, P1229 Licence.

http://og.decc.gov.uk/en/olgs/cms/licences/licence_relinq/relinquishment/relinquishment/relinquishment.aspx

Doornenbal, H. & Stevenson, A. (eds) 2010. *Petroleum Geological Atlas of the Southern Permian Basin Area*. Houten, Netherlands, EAGE.

Evans, C.J. & Brereton, N.R. 1990. In situ crustal stress in the United Kingdom from borehole breakouts. *In: Hurst, A., Lovell, M.A. & Morton, A.C. (eds) Geological applications of wireline logs*, Geological Society, London, Special Publications, **48**, 327–338.

Fejerskov, M. & Lindholm, C. 2000. Crustal stress in and around Norway: an evaluation of stress-generating mechanisms. *In: Nottvedt, A. (ed.) Dynamics of the Norwegian Margin*, Geological Society, London, Special Publications, **167**, 451–467.

Fisher, M.J. 1984. Triassic. *In: Glennie, K.W. (ed.) Introduction to the Petroleum Geology of the North Sea*, Blackwell Scientific Publications, Oxford, 113–132.

Glennie, K.W. & Boegner, P.L.E. 1981. Sole Pit Inversion Tectonics. *In*: Illing, L.V. & Hobson, G.D. (eds) *Petroleum Geology of the Continental Shelf of North-west Europe – Proceedings of the Second Conference on Petroleum Geology of the Continental Shelf of North-West Europe*, Heyden and Son Ltd, London, 110–120.

Griffiths, P.A., Allen, M.R., Craig, J., Fitches, W.R. & Whittington, R.J. 1995. Distinction between fault and salt control of Mesozoic sedimentation on the southern margin of the Mid-North Sea High. *In*: Boldy, S.A.R. (ed.) *Permian and Triassic Rifting in Northwest Europe*, Geological Society, London, Special Publications, **91**, 145–159.

Heidbach, O., Tingay, M., Barth, A., Reinecker, J., Kurfeß, D. & Müller, B. 2008. The World Stress Map database release 2008 doi:10.1594/GFZ.WSM.Rel2008.

Heinemann, N., Wilkinson, M., Pickup, G.E., Haszeldine, R.S. & Cutler, N.A. 2012. CO₂ storage in the offshore UK Bunter Sandstone Formation. *International Journal of Greenhouse Gas Control*, **6**, 210–219.

Hillis, R.R. & Nelson, E.J. 2005. *In situ* stresses in the North Sea and their applications: petroleum geomechanics from exploration to development. *In*: Doré, A.G. & Vining, B.A. (eds) *Petroleum Geology: North-West Europe and Global Perspectives – Proceedings of the 6th Petroleum Geology Conference*, Geological Society, London, 551–564.

Holloway, S., Vincent, C.J., Bentham, M.S. & Kirk, K.L. 2006. Top-down and bottom-up estimates of CO₂ storage capacity in the UK sector of the Southern North Sea Basin. *Environmental Geoscience*, **13**, (2), 74–81.

IPCC 2005. *Special Report on Carbon Dioxide Capture and Storage*. Metz, B., Davidson, O., de Coninck, H.C., Loos, M. & Meyer, L.A. (eds) Cambridge University Press, Cambridge.

Ketter, F.J. 1991. The Esmond, Forbes and Gordon Fields, Blocks 43/8a, 43/13a, 43/15a, 43/20a, UK North Sea. *In*: Abbotts, I.L. (ed.) *United Kingdom Oil and Gas fields, 25 Years Commemorative Volume*, Geological Society, London, Memoir 14, 425–432.

Lott, G.K. & Knox, R.W.O'B. 1994. Post-Triassic of the Southern North Sea. *In*: Knox, R.W.O'B. & Cordey, W.G. (eds) *Lithostratigraphic nomenclature of the UK North Sea*, British Geological Survey, Nottingham.

Morone, C. 1995. Fault zone strength and failure criteria. *Geophysical Research Letters*, **22** (6), 723–726.

Morris, A., Ferrill, D.A. & Henderson, D.B. 1996. Slip-tendency analysis and fault reactivation. *Geology*, **24** (3), 275–278.

Naylor, M., Wilkinson, M. & Haszeldine, R.S. 2011. Calculation of CO₂ column heights in depleted gas fields from known pre-production gas column heights. *Marine and Petroleum Geology*, **28**, 1083–1093.

Noy, D.J., Holloway, S., Chadwick, R.A., Williams, J.D.O., Hannis, S.D. & Lahann, R.W. 2012. Modelling large-scale carbon dioxide injection into the Bunter Sandstone in the UK Southern North Sea. *International Journal of Greenhouse Gas Control*, **9**, 220–233.

Ritchie, J.S. & Pratsides, P. 1993. The Caister fields, Block 44/23a, UK North Sea. *In*: Parker, J.R. (ed.) *Petroleum Geology of Northwest Europe: Proceedings of the Fourth Conference*, Geological Society, London, 759–769.

Samuelson, J. & Spiers, C.J. 2012. Fault friction and slip stability not affected by CO₂ storage: Evidence from short-term laboratory experiments on North Sea reservoir sandstones and caprocks. *International Journal of Greenhouse Gas Control*, **115**, 578–590.

Schroot, B.M. & Schüttenhelm, R.T.E. 2003. Expressions of shallow gas in the Netherlands North Sea. *Geologie en Mijnbouw*, **82** (1), 91–105.

Schroot, B.M., Klaver, G.T. & Schüttenhelm, R.T.E. 2005. Surface and subsurface expressions of gas seepage to the seabed – examples from the Southern North Sea. *Marine and Petroleum Geology*, **22**, 499–515.

Seedhouse, J.K. & Racey, A. 1997. Sealing capacity of the Mercia Mudstone Group in the East Irish Sea Basin: Implications for petroleum exploration. *Journal of Petroleum Geology*, **20** (3), 261–286.

Spain, J.D. & Conrad, C.P. 1997. Quantitative analysis of top-seal capacity: offshore Netherlands, Southern North Sea. *Geologie en Mijnbouw*, **76** (3), 217–226.

Stewart, S.A. & Coward, M.P. 1995. Synthesis of salt tectonics in the southern North Sea, UK. *Marine and Petroleum Geology*, **12** (5), 457–475.

Streit, J.E. & Hillis, R.R. 2004. Estimating fault stability and sustainable fluid pressures for underground storage of CO₂ in porous rock. *Energy*, **29**, 1445–1456.

Taylor, J.C.M. 1984. Late Permian – Zechstein. *In: Glennie, K.W. (ed.) Introduction to the Petroleum Geology of the North Sea*, Blackwell Scientific Publications, Oxford, 87–111.

Teufel, L.W. 1991. Influence of lithology and geologic structure on in situ stress: Examples of stress heterogeneity in reservoirs. *In: Lake, L.W., Carroll, H.B. & Wesson, T.C. (eds) Reservoir Characterization II*, Academic Press, San Diego. 565–579.

Underhill, J.R. 2003. The tectonic and stratigraphic framework of the United Kingdom's oil and gas fields. *In: Gluyas, J.G. & Hitchens, H.M. (eds) United*

Kingdom Oil and Gas Fields, Commemorative Millennium Volume, Geological Society, London, Memoir 20, 17–59.

Underhill, J.R. 2009. Role of intrusion-induced salt mobility in controlling the formation of the enigmatic ‘Silverpit Crater’, UK Southern North Sea. *Petroleum Geoscience*, **15**, 197–216.

Underhill, J.R., Lykakis, N. & Shafique, S. 2009. Turning exploration risk into a carbon storage opportunity in the UK Southern North Sea. *Petroleum Geoscience*, **15**, 291–304.

Van Hoorn, B. 1987. Structural evolution, timing and tectonic style of the Sole Pit inversion. *Tectonophysics*, **137**, 239–284.

Wall, M., Cartwright, J., Davies, R. & McGrandle, A. 2009. 3D seismic imaging of a Tertiary Dyke Swarm in the Southern North Sea, UK. *Basin Research*, **22** (2), 181–194.

Warren, J.K. 2006. *Evaporites: Sediments, Resources and Hydrocarbons*. Springer Berlin Heidelberg, New York.

Williams, J.D.O., Jin, M., Bentham, M., Pickup, G.E., Hannis, S.D. & Mackay, E.J. 2013. Modelling carbon dioxide storage within closed structures in the UK Bunter Sandstone Formation. *International Journal of Greenhouse Gas Control*, **18**, 38–50.

Yielding, G., Freeman, B. & Needham, D.T. 1997. Quantitative Fault Seal Prediction. *AAPG Bulletin*, **81** (6), 897–917.

Yielding, G., Lykakis, N. & Underhill, J.R. 2011. The role of stratigraphic juxtaposition for seal integrity in proven CO₂ fault-bound traps of the Southern North Sea. *Petroleum Geoscience*, **17**, 193–203.

Zoback, M.D., Barton, C.A., Brudy, M., Castillo, D.A., Finkbeiner, T., Grollimund, B.R., Moos, D.B., Peska, P., Ward., C.D. & Wiprut, D.J. 2003. Determination of stress orientation and magnitude in deep wells. *International Journal of Rock Mechanics & Mining Sciences*, **40**, 1049–1076.

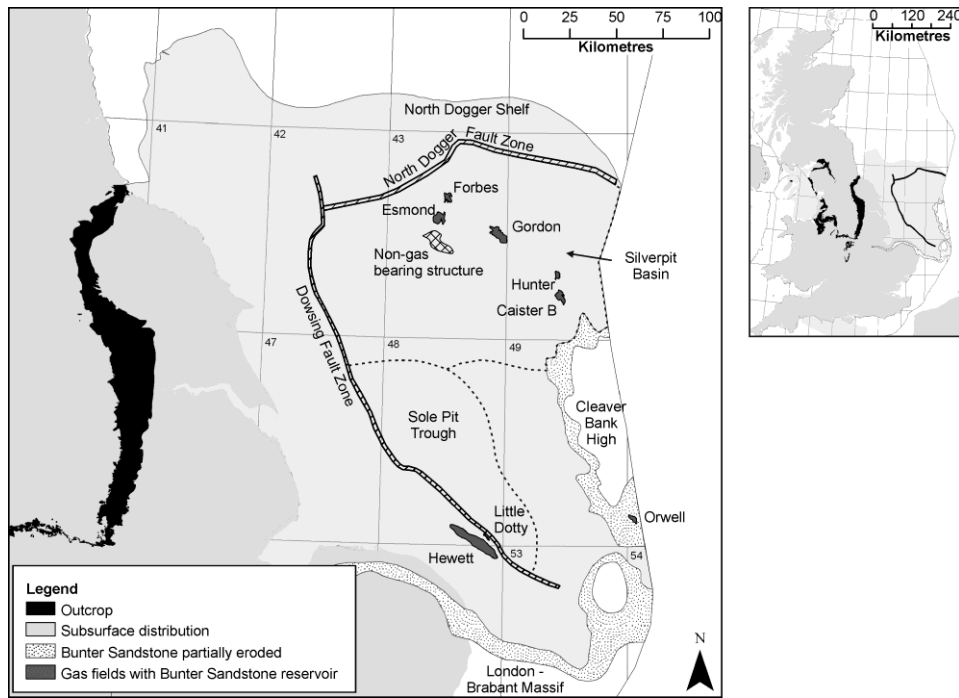


Fig. 1. Gas fields and structures referred to herein, developed in the UK Southern North Sea BSF. The locations of the Dowsing and North Dogger Fault Zones are approximate; they are each composed of several individual, commonly en echelon faults.

CHRONO-STRATIGRAPHY		LITHOSTRATIGRAPHY			
CENOZOIC	QUATERNARY	Nordland Group			
	NEOGENE	Base Miocene Unconformity			
	PALAEOGENE	Undifferentiated			
MESOZOIC	CRETACEOUS	Late	Chalk Group	Undifferentiated	
		Early	Cromer Knoll Group	Red Chalk Fm.	
				Speeton Clay Fm.	
	JURASSIC	Late Cimmerian Unconformity			
	TRIASSIC	Late	Humber, West Sole & Lias Groups		
			Penarth Group		
		Early	Bacton Group	Haisborough Group	
				Undifferentiated	
	PALAEOZOIC	PERMIAN	Late	Zechstein Group	
			Early	Rottliegend Gp.	Silverpit Fm. & Leman Sandstone Fm.
CARBONIFEROUS		Late	Base Permian Unconformity		
			Conybeare Group		

Fig. 2. Generalised stratigraphy of UK sector Southern North Sea.

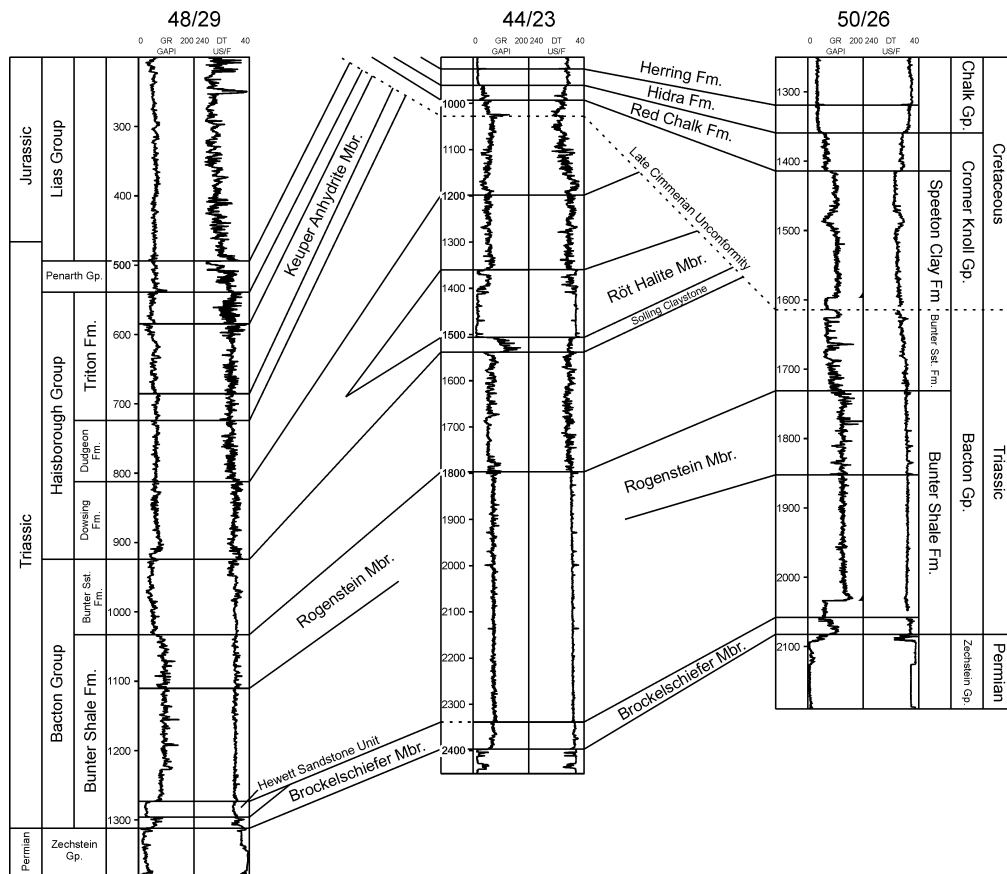


Fig. 3. Representative well log response of the BSF (highlighted) and immediately over- and underlying seals. Well from block 48/29 is representative of the stratigraphy in the Hewett and Little Dotty fields, 44/23 is representative of the Hunter Field, while 50/26 is representative of the stratigraphy of the Orwell Field.

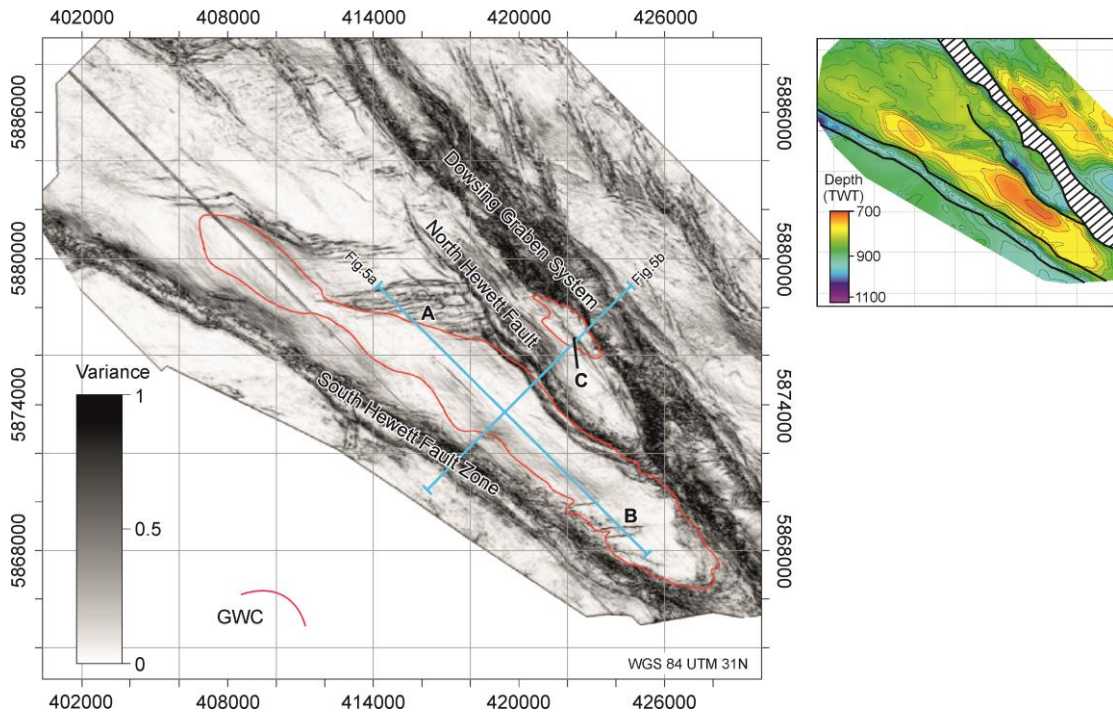


Fig. 4. Variance display of the top BSF surface in the Hewett and Little Dotty gas fields, and depth to top BSF (inset). GWC: approximate initial gas-water contact in the Hewett and Little Dotty gas fields. Labelled faults indicate those marked on Figure 5. Data courtesy of Tullow Oil.

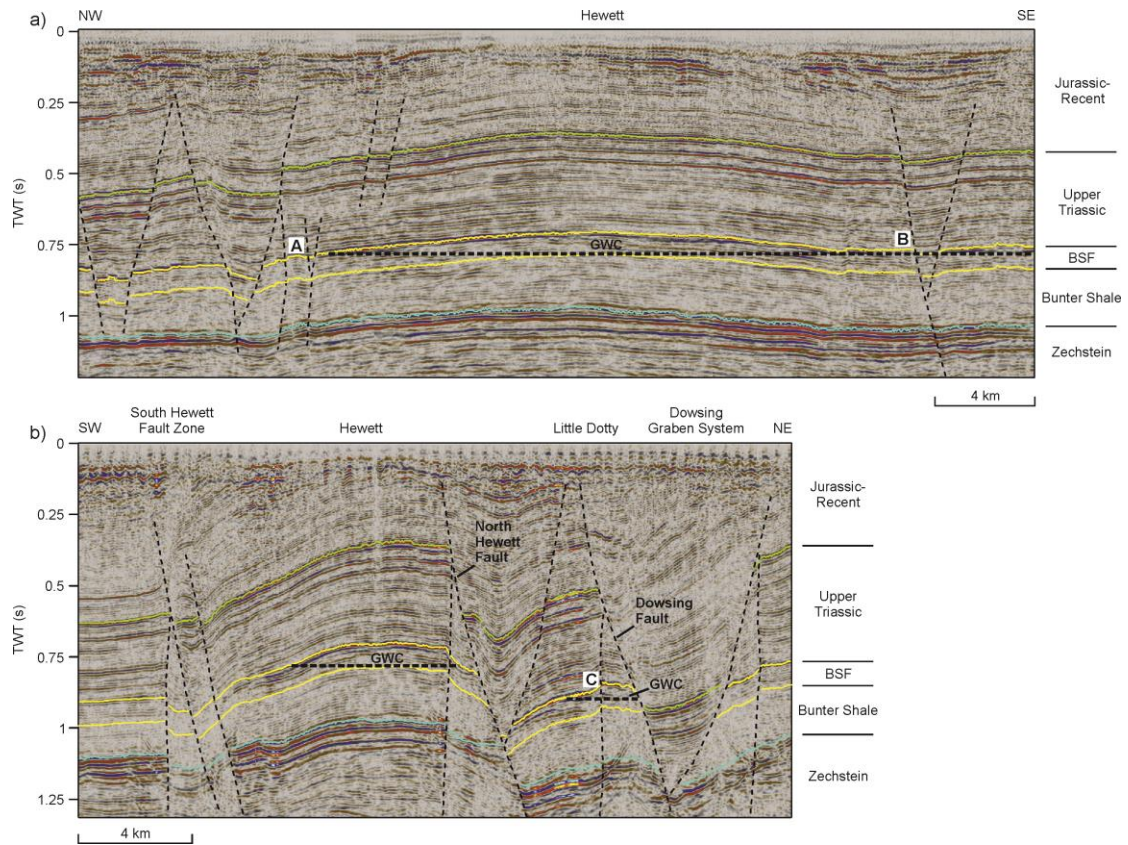


Fig. 5. Seismic sections through the Hewett Field, (a) illustrating faults cutting the BSF, and (b) faults cutting the BSF in the Hewett and Little Dotty gas fields. Location of seismic lines are indicated on Figure 4. Data courtesy of Tullow Oil.

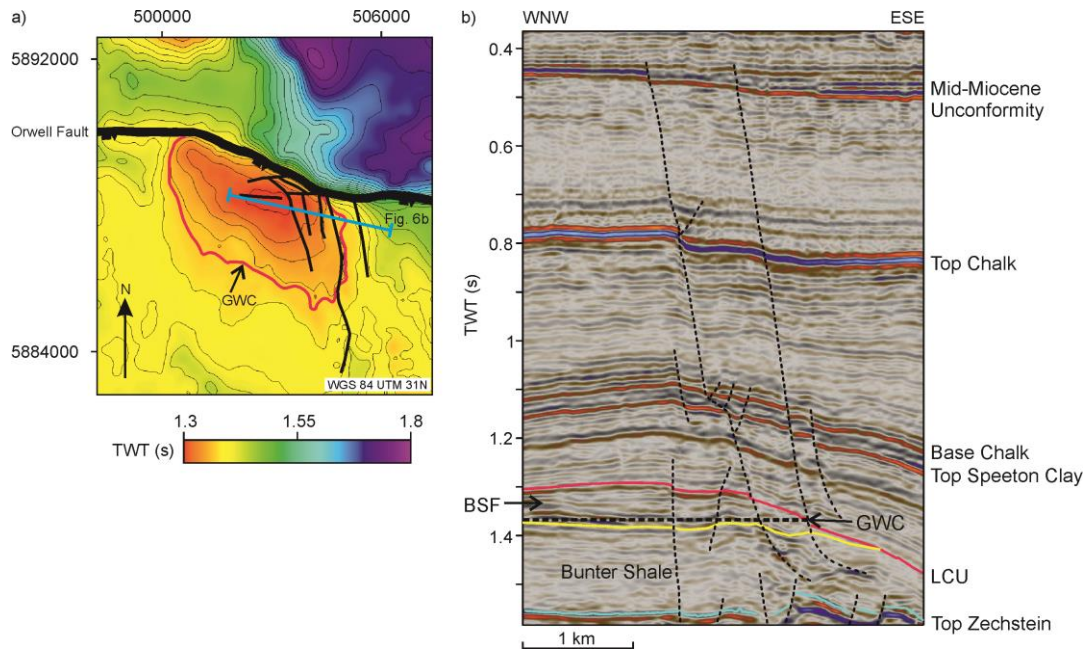


Fig. 6. The Orwell Field, Block 50/26. (a) Structure contour map of the LCU, showing the approximate location of the pre-production Orwell GWC. (b) Seismic reflection section through part of the Orwell Field, showing the relationship between the pre-production GWC and faulting. Data courtesy of Tullow Oil.

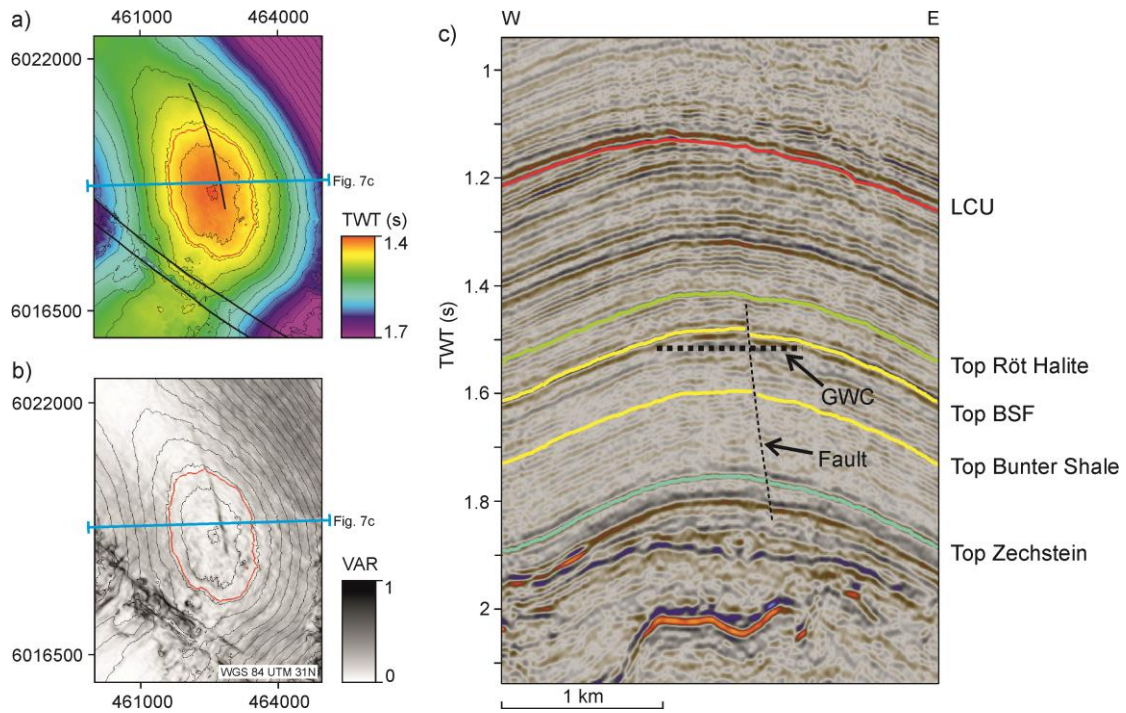


Fig. 7. The Hunter Field, Quadrant 44. (a) Depth to top BSF surface over the Hunter Field showing approximate location of GWC (red outline) in relation to faults cutting the BSF. (b) Variance display of the top BSF surface. (c) Seismic reflection section through the Hunter Field showing relationship between faults and interpreted initial GWC. SNS MegaSurvey data courtesy of PGS.

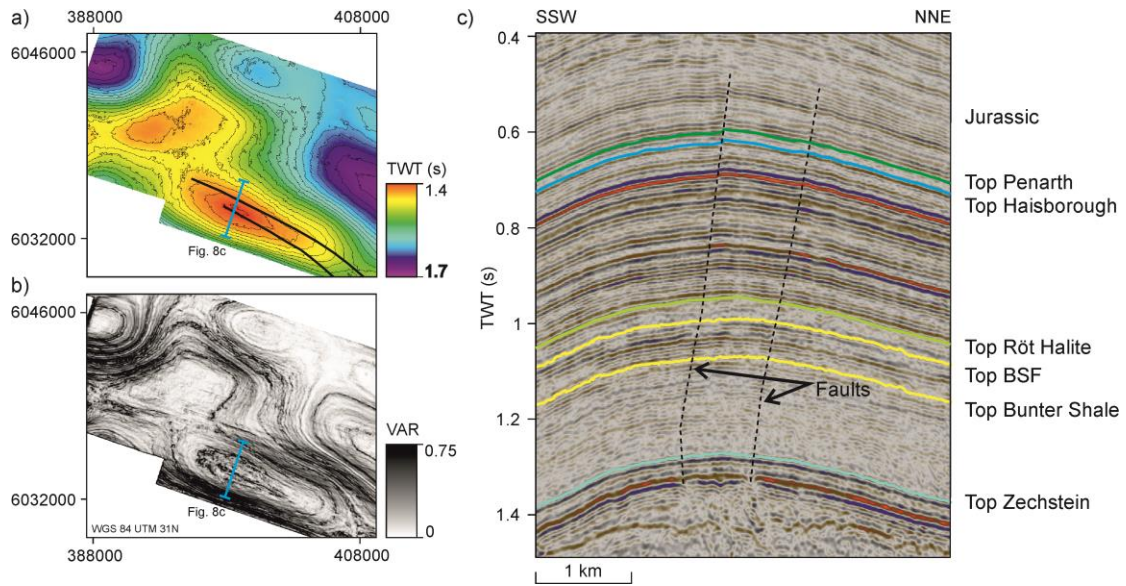


Fig. 8. Illustration of a non-gas bearing structure in Quadrant 43, (a) structure map at the level of the top BSF surface, (b) Seismic Variance map on a time-slice near the crest of the structure, showing the location of two faults along the structural axis. The two faults pass down through the BSF reservoir at least into the upper part of the Zechstein Group, and upwards into the Jurassic strata. (c) Seismic reflection section across the structure. Seismic data shown courtesy of WesternGeco.

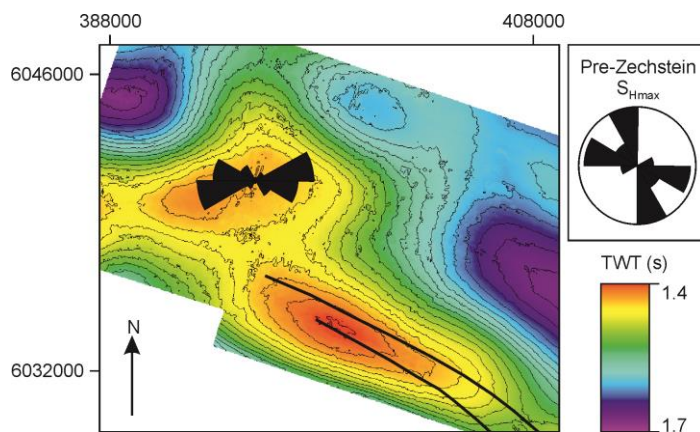


Fig. 9. Orientation of S_{Hmax} over the non-gas bearing structure in Quadrant 43, derived from analysis of borehole breakouts in well 43/12-1. The rose diagram is plotted at the well location on the structure, and shows the orientation of S_{Hmax} in the post-salt

succession, while the outer rose diagram shows the S_{Hmax} orientation in the pre-Zechstein strata.

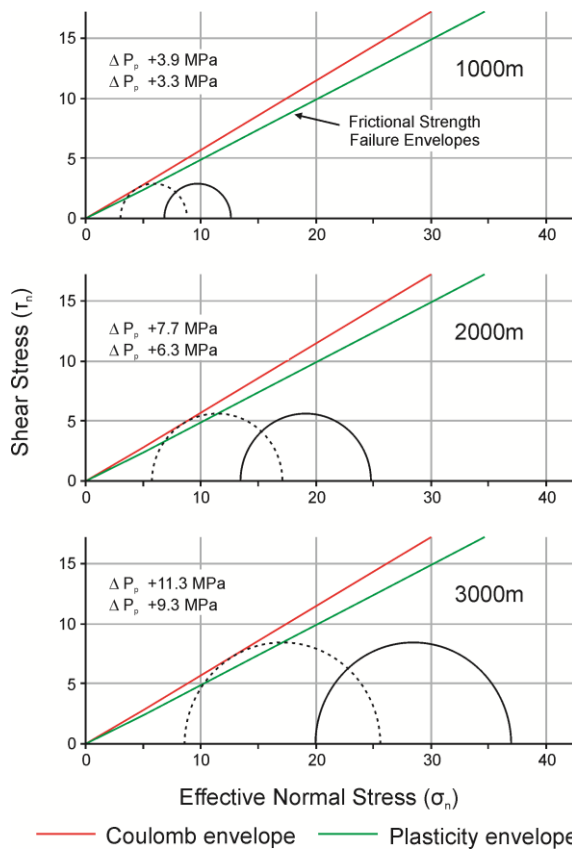


Fig. 10. Mohr-Coulomb diagrams indicating the pore fluid pressure (ΔP_p) increase required to cause frictional failure of pre-existing, optimally oriented cohesionless faults at various depths. The solid Mohr-circles represent the assumed pre-injection state of stress, while the dotted Mohr-circles illustrate the effect of raising the pore fluid pressure up to the Coulomb fault failure envelope. ΔP_p values are given for both the Coulomb (upper) and Coulomb-Plasticity failure envelopes.

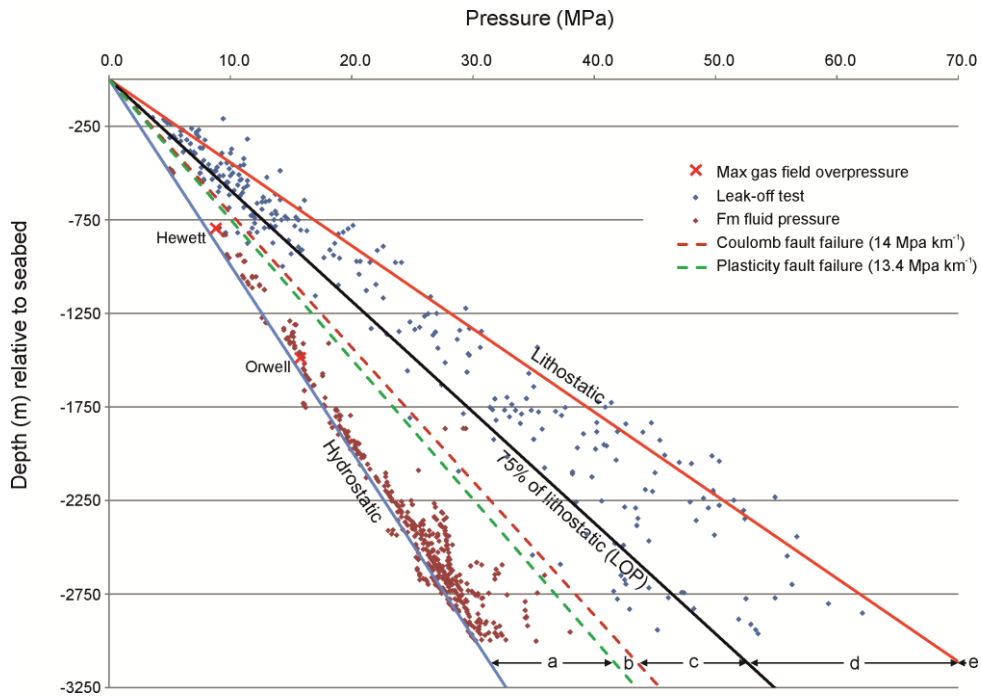


Fig. 11. Pressure data from the SNS, showing the relationship between the hydrostatic, lithostatic, LOP and modelled fault failure (reactivation) gradients. It is possible that LOP values falling between the various pressure gradients are influenced by the following factors: Tests not being fully taken to leak-off (a), reactivation of optimally oriented faults (b), reactivation of non-optimally oriented faults (c), failure of intact rock (d), or local variations of the lithostatic pressure gradient and spurious LOP measurements (e). Pressure data courtesy of IHS, reproduced from Noy *et al.* (2012).

Field	Depth to crest (TVDSS m)	GIIP (bcm)	Column height (m)	Source
Hewett	792.5	38.4	128	Cooke-Yarborough & Smith 2003
Little Dotty	1067.1	2.8	50.6	Cooke-Yarborough & Smith 2003
Esmond	1258.5	10.8	36	Bifani 1986; Ketter 1991
Forbes	1697.6	2.9	88	Bifani 1986; Ketter 1991
Gordon	1527.4	5.2	57	Bifani 1986; Ketter 1991
Caister B	1325	4.4	75	Ritchie & Pratsides 1993
Hunter	1836.5	Unreported	60.5	Well 44/23a-10
Orwell	1500	8	101.4	Well 50/26a-D1

Table 1. *Depths to crest of producing fields and volumes of gas initially-in-place.*

Parameter	Value	Source
Maximum principal stress gradient (assumed to be vertical)	22.5 MPa km ⁻¹	Lithostatic pressure gradient (Noy <i>et al.</i> 2012)
Conservative minimum horizontal stress gradient	16.9 MPa km ⁻¹	Minimum LOP gradient, corresponding to 75% of the lithostatic pressure gradient (Noy <i>et al.</i> 2012)
Fault orientation	30° to S _{max}	Assumed to be optimally oriented
Hydrostatic pressure gradient (virgin pore-fluid pressure)	10.07 MPa km ⁻¹	Noy <i>et al.</i> 2012
Coefficient of friction of faults	0.56	Short-term laboratory experiments using simulated fault gouge (Samuelson & Spiers 2012)

Table 2. *Parameters and their sources used for geomechanical modelling.*